Title

Demonstration of motion-resistant three-wavelength spatial frequency domain imaging system with ambient light suppression using an 8-tap CMOS image sensor

ISBN

9781510658578

Authors

Feng, Yu

Shimada, Yuto

Cao, Chen

et al.

Publication Date

2023-03-07

DOI

10.1117/12.2649418

Demonstration of motion-resistant three-wavelength spatial frequency domain imaging system with ambient light suppression using an 8-tap CMOS image sensor

Yu Feng*[a], Yuto Shimada[a], Chen Cao[b], Keita Yasutomi[b], Shoji Kawahito[b]
Gordon T. Kennedy[c], Anthony J. Durkin[c, d], and Keiichiro Kagawa[b]
[a]Graduate School of Integrated Science and Technology, Shizuoka University
[b]Research Institution of Electronics, Shizuoka University
[c]Beckman Laser Institute, University of California, Irvine
[d]Biomedical Engineering Department, University of California, Irvine

ABSTRACT

We demonstrate a motion-resistant, three-wavelength, spatial frequency domain imaging (SFDI) system with ambient light suppression using a new 8-tap CMOS image sensor developed in our laboratory. Compared to the previous sensor (134×150), the new sensor's readout maximum frame rate has improved to 33fps from 6.28fps, and the new 700×540-pixel sensor allows imaging at a higher spatial resolution over a larger field of view. Furthermore, the number of projected images needed per wavelength is reduced from three to two after applying the Hilbert transform. One image of planar illumination and one image for sinusoidal pattern projection at three wavelengths as well as one image of ambient light are captured by the 8-tap image sensor concurrently. The bias caused by ambient light is removed by subtracting the ambient light image from other images. Suppression of motion artifacts is achieved by reducing the exposure and projection time of each pattern. Sufficient signal level is maintained by repeating the exposure multiple times. In this study, LEDs with wavelengths of 554nm, 660nm, and 730nm were used to estimate oxy-/deoxyhemoglobin and melanin concentrations from in-vivo volar forearm skin.

Keywords: Spatial frequency domain imaging, diffuse optics, multi-spectral imaging, multi-tap CMOS image sensor

1. INTRODUCTION

Spatial frequency domain imaging (SFDI) is a wide-field imaging technique that projects structured light of different spatial frequencies and phases onto biological tissues to quantify absorption and reduced scattering coefficients[1]. We demonstrate a motion-resistant three-wavelength, SFDI system with ambient light suppression. The device uses a new laboratory-designed 8-tap CMOS image sensor and the Hilbert transform.

SFDI can help assess burn severity at an early stage since scattering changes with the burn severity and the measurement results from laser Doppler and laser speckle contrast imaging are not accurate due to vasoconstriction at that stage. However, one of the drawbacks of SFDI is that the projection can be affected by ambient light. In addition, subject motion can also cause an error in measurement since a set of patterns is projected sequentially.

We present a three-wavelength spatial frequency domain imaging system with our new 8-tap image sensor[2]. Compared to the previous sensor with 134×150 pixels, the new 700×540-pixel sensor allows imaging at a higher spatial resolution over a larger field. Furthermore, the new sensor's readout frame rate has improved to 33fps from the previous 6.28fps. Our 8-tap image sensor-based imaging system can capture multiple images at the in-pixel storage diodes in the charge domain and can implement different exposures simultaneously[3]. Although SFDI typically utilizes three phases, the number of the images needed per wavelength is reduced to two after applying the Hilbert transform, since we can obtain the cosine images from sine images by calculation[4]. Since our 8-tap image sensor can capture eight images simultaneously, by applying the Hilbert transform, our sensor is suitable for three-wavelength SFDI. One image for planar illumination and one image for sinusoidal pattern projection on the tissue at three wavelengths and one image of ambient light are captured concurrently. The bias caused by ambient light is removed by subtracting the ambient light image from other images. Suppression of motion artifacts is achieved by reducing the exposure and projection time of each pattern to 1/N. Sufficient signal level is maintained by repeating the exposure N times. Due to the technical restriction of the digital mirror device (DMD), the repetition number is set to three in this study. In this study, LEDs with the wavelengths of 554nm, 660nm, and 730nm

Optical Tomography and Spectroscopy of Tissue XV, edited by Sergio Fantini, Paola Taroni, Proc. of SPIE Vol. 12376, 123760D · © 2023 SPIE
1605-7422 · doi: 10.1117/12.2649418

were used for tissue measurement. By using this combination of wavelengths, we expect to be able to quantify oxy and deoxyhemoglobin on a pixel by pixel basis, as well as the reduced scattering coefficient at each of these wavelengths.

High-frame-rate cameras can also perform motion artifact suppression and ambient light removal. However, the high-frame-rate cameras will put out a large amount of data, which require large computation capability, and cause higher read noise due to wider noise bandwidth. For most tissue measurement application, video rates (~10fps) are sufficient. Therefore, frame rates greater than the video rate is not necessary. By comparison, multiple exposure with our 8-tap image sensor results in fewer images to read and, less read noise than high-frame-rate cameras. Our method is promising in the sense that motion artifacts and ambient light bias suppression at video rates can be achieved. In this paper, the principle of 8-tap CMOS image sensor and the Hilbert transform based three-band SFDI is presented.

2. THEORY OF SFDI WITH MULTI-TAP CMOS IMAGE SENSOR

2.1. Multi-tap CMOS image sensor

Multi-tap CMOS image sensor pixel with the lateral electric filed charge modulator (LEFM) has been developed for short-pulse based time-of-flight depth imaging, as described in Ref. 3. LEFM enables ultrafast charge transfer and made increasing the number of taps possible[5]. Fig. 1 shows the structure and function of a 2-tap charge modulator pixel with charge draining. The pixel's taps can be controlled separately by the corresponding Transfer gates (TGs). During the accumulation period, when one of the taps is active, i.e., TG is on, due to the potential lowered by the TG, the photo-generated charges are transferred to the corresponding tap and stored in the storage diode (SD). Since the TG can turn on and off multiple times within the accumulation period, multiple exposure is possible with multi-tap pixels. During the readout period, the amount of the charges in SDs are read separately. Thus, two images are obtained from the sensor. The function of the 8-tap image sensor's pixel used in our imaging system is depicted in Fig. 2. With an 8-tap image sensor, eight images are obtained after readout.

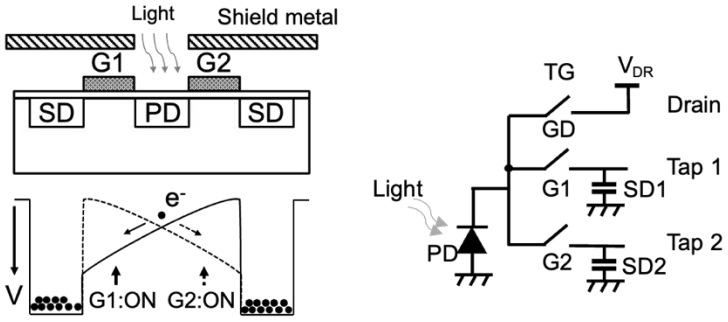

(a) (b)

Figure 1. (a) Structure of 2-tap LEFM pixel with the charge drain, (b) Schematic diagram of 2-tap LEFM pixel

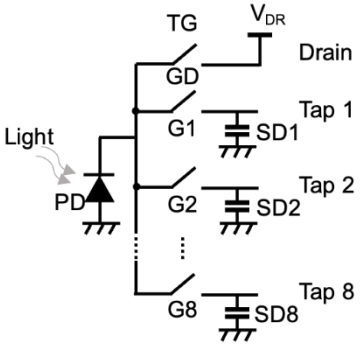

Figure 2. Schematic diagram of 8-tap LEFM pixel with the charge drain.

2.2. Estimating absorption and reduced scattering coefficient by SFDI

Typically, in SFDI, planar (DC) and sinusoidal (AC) patterns are projected onto the sample and the reflectance images are captured by a camera, as shown in Fig. 3. The projected AC pattern, S can be denoted in Eq. 1, where S_0, M_0, f_x, and α are the illumination source intensity, modulation depth, spatial frequency, and spatial phase, respectively[6].

$$S = \frac{S_0}{2}[1 + M_0 \cos(2\pi f_x x + \alpha)]. \quad (1)$$

The reflected intensity, I is the sum of DC component I_{DC} and AC component I_{AC}, denoted as

$$\begin{aligned} I(x, f_x) &= I_{DC}(x) + I_{AC}(x, f_x) \\ &= M_{DC}(x) + M_{AC}(x, f_x) \cdot \cos(2\pi f_x x + \alpha), \end{aligned} \quad (2)$$

where $M_{DC}(x)$ stands for the DC reflectance at position x, and $M_{AC}(x, f_x)$ stands for the AC reflectance of spatial frequency f_x at position x. Here, we employ the single-pixel demodulation method, where three phase-shifted patterns with the same special frequency are projected onto the sample sequentially. M_{DC}, M_{AC} can then be calculated at each pixel.

In this study, one DC pattern and two AC patterns, with phase offsets α=0 and π/2 radians are selected. $M_{DC}(x)$, $M_{AC}(x, f_x)$ can then be calculated at each location x by

$$M_{DC}(x) = I_{DC}(x), \quad (3)$$

$$M_{AC}(x, f_x) = \sqrt{(I_0 - I_{DC})^2 + (I_{\frac{\pi}{2}} - I_{DC})^2}, \quad (4)$$

where I_{DC}, I_0, and $I_{\frac{\pi}{2}}$ are the pixel value of each corresponding reflectance image at the position x. Since the measured result includes the effects of the light source intensity, f-number of lens, and so on. To obtain the sample's reflectance, the measured result needs to be calibrated by the reference measurement of a tissue-mimicking phantom with known optical properties. The calibrated reflectance $M_{DC,cal}$ and $M_{AC,cal}$ are expressed as

$$M_{DC,cal} = M_{DC}(x) \times \frac{M_{DC0,ref}(x)}{M_{DC,ref}(x)}, \quad (5)$$

$$M_{AC,cal} = M_{AC}(x, f_x) \times \frac{M_{AC0,ref}(x, f_x)}{M_{AC,ref}(x, f_x)}, \quad (6)$$

where $M_{DC,ref}, M_{AC,ref}$ are the measured pixel values obtained from the camera for the reference phantom, and $M_{DC0,ref}, M_{AC0,ref}$ are the simulated reflectance values of the reference phantom calculated by Monte Carlo simulation.

Using the calibrated reflectance, $M_{DC,cal}$ and $M_{AC,cal}$, the absorption and reduced scattering coefficients, μ_a and μ_s' of the sample are estimated by referencing a look-up table (LUT), which is generated by the Monte Carlo simulation based on a two-layered skin mode, as shown in Fig.4. In this model, we assumed that melanin is distributed in the epidermis and hemoglobin in the dermis.

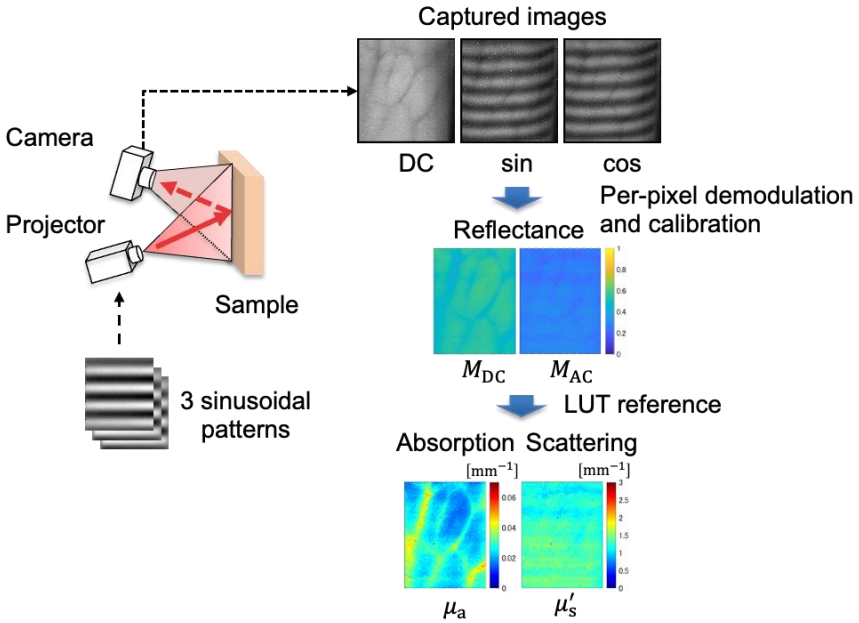

Figure 3. Image acquisition flow of SFDI: Phase-shifted patterns are projected onto the sample sequentially. To obtain the sample's reflectance, the reflectance images captured by the camera are then demodulated and calibrated at each pixel. Sample's absorption and reduced scattering coefficients are then estimated by referencing a look-up-table generated by Monte Carlo simulation.

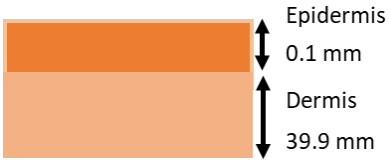

Figure 4. Schematic diagram of the two-layer model.

2.3. Estimating chromophore concentrations and scattering parameters by multi-band SFDI

Biochromophores in tissue such as oxygenated hemoglobin, deoxygenated hemoglobin, melanin, water have different absorption spectra and the concentration of which can be estimated by using Beer–Lambert law. The absorption coefficient μ_a at a certain wavelength, λ, can be characterized by

$$\mu_a(\lambda) = \ln(10) \cdot \sum_n \varepsilon_n(\lambda) \cdot c_n, \tag{7}$$

where c_n and $\varepsilon_n(\lambda)$ represent the concentration and molar absorbance of biochromophores[7]. In multi-band SFDI, the absorption coefficient μ_a are measured at multiple wavelengths, along with the known molar absorbance of each biochromophores at a certain wavelength, the concentrations of each biochromophores can be estimated by

$$\begin{bmatrix} \mu_a(\lambda_1) \\ \vdots \\ \mu_a(\lambda_j) \end{bmatrix} = \ln(10) \cdot \begin{bmatrix} \varepsilon_1(\lambda_1) & \cdots & \varepsilon_i(\lambda_1) \\ \vdots & \ddots & \vdots \\ \varepsilon_1(\lambda_j) & \cdots & \varepsilon_i(\lambda_j) \end{bmatrix} * \begin{bmatrix} c_1 \\ \vdots \\ c_i \end{bmatrix}, \tag{8}$$

where i represent the number of biochromophores and j is the number of measured wavelengths. Note that $j \geq i$ is needed to separate the concentrations of biochromophores.

In tissue measurement, total hemoglobin c_{tHB} and tissue oxygen saturation StO_2 are the most important indicators of good health, which are denoted by

$$c_{tHB} = c_{o_2Hb} + c_{HHb}, \tag{9}$$

$$StO_2 = \frac{c_{o_2Hb}}{c_{o_2Hb} + c_{HHb}}, \tag{10}$$

Multi-band SFDI also have the benefit of obtaining reduced scattering coefficient μ_s' for multiple wavelengths. The scattering parameters, a and b, can be obtained by fitting the measured reduced scattering coefficients at multiple wavelengths with the following:

$$\mu_s'(\lambda) = a\left(\frac{\lambda}{500\ \text{nm}}\right)^{-b}. \tag{11}$$

where a is the scattering amplitude normalized to 500 nm and b is the scattering power. The scattering parameters are useful parameters in burn severity diagnosis since a and b change drastically depending on the burn severity[8].

2.4. Suppressing ambient light bias and motion artifacts in SFDI using multi-tap CMOS image sensors

In the multi-tap CMOS image sensor based SFDI, the control signals for the light source, DMD based projector, and the sensor are synchronized. Each one of the projected patterns at different wavelengths is assigned to and captured by one of the taps of the multi-tap image sensor. To eliminate the DC bias caused by ambient light, one of the taps is assigned to capture the sample without any pattern projection, i.e., the ambient light. The image for the ambient light is subtracted from other images with pattern projection. To suppress motion artifacts in SFDI measurement, the time for each pattern projection and sensor exposure can be shortened, such that the movement between each frame are not visible. Shortened pattern projection and sensor exposure comes with a drawback that the light intensity decreases, therefore, signal-to-noise ratio worsens. Since multiple exposure is possible with multi-tap sensor, repeating such shortened pattern projection and sensor exposure, the light intensity can be maintained, as shown in Fig. 5.

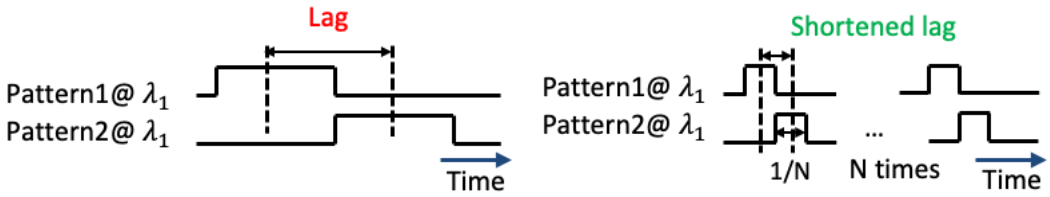

(a) (b)

Figure 5. Temporal lags are shortened while maintaining light intensity by reducing the pattern projection and sensor exposure time and repeating the process N times. (a) single exposure, (b) repeat N times

3. METHODS

3.1. Hilbert transform

To measure the metabolic information of tissue, the concentrations of oxy-/deoxy-hemoglobin are needed, which requires measurement at more than two wavelengths. However, melanin existing in the epidermis has higher molar absorbance than other chromophores, meaning that for accurate tissue measurement, measurement for at least three wavelengths (one for each chromophore) is necessary. Typically, SFDI requires three images, each shifted by 120° for each wavelength. However, the number of taps is difficult to increase more than eight, as it will result in larger pixel size and smaller photosensitive areas in the pixel. As demonstrated in Ref. 4, the Hilbert transform is useful to reduce the number of projection patterns per wavelength needed in SFDI. In this study, we reduce the number of projection patterns per wavelength from three to two and measure at more than three wavelengths with the 8-tap image sensor, as it is possible to obtain a phase-shifted by $\pi/2$ rad signal by Hilbert transform, i.e., calculating the cosine signal from a sine signal.

3.2. Three-wavelengths SFDI with 8-tap image sensor

Table 1 shows the example projection patterns at each wavelength and the corresponding tap number.

Table 1. Example projection patterns in our SFDI system

λ of LED	λ_1(554nm)		λ_2(660nm)		λ_3(730nm)		λ_4(850nm)	Ambi-ent
Pattern	DC	sin	DC	sin	DC	sin	DC	
Captured images								
Tap#	1	2	3	4	5	6	7	8

Images for the cosine patterns are then calculated from images for the sine patterns by the Hilbert transform. Tap-7 captures an DC image for an additional wavelength. Tap-8 captures the ambient light image for removing bias caused by ambient light. M_{DC} and M_{AC} are obtained by demodulation and calibration. μ_a and μ_s' maps are estimated by referring to the LUT. Thereafter, biochromophore concentrations and scattering parameters are estimated as mentioned in Sec. 2.3.

4. EXPERIMENT

4.1. Experimental instrumentation

Table 2 shows the specifications of our new 8-tap image sensor, while Fig. 6 shows the optics of our system. The measured sample is a human forearm under a dark room environment. The spatial frequency of the projected patterns was 0.10 mm^{-1}. Exposure was repeated three times. The time for each pattern projection and sensor exposure were chosen as 3ms. Therefore, compared to the read-out frame rate 33fps, the frame rate of our SFDI system is 9.4fps. Although shorter projection time (higher frame rate) is possible with the DMD, shorter projection time will result in higher quantization noise in the projected pattern. To suppress the dark current of the sensor, the result image was an average of 10 images. Fig. 7 shows the measured image (average of 10 images) of our SFDI system. DC, sine images for the three main wavelengths, and one additional DC image for the 4th wavelength and one image for ambient light were captured simultaneously.

Table 2. Specifications of the 8-tap image sensor

Pixel size	12.6 × 12.6 [μm^2]
Pixel number	700(H) × 540(V)
Tap number	8 taps + Drain
Frame rate	9.4fps

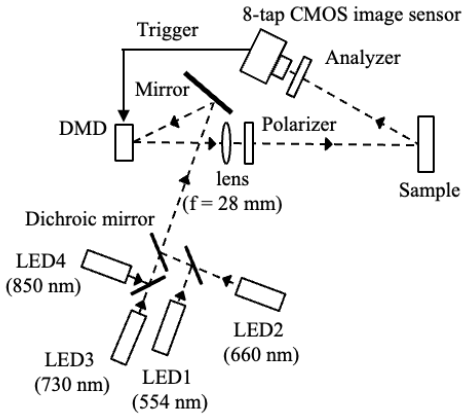

Figure 6. System setup.

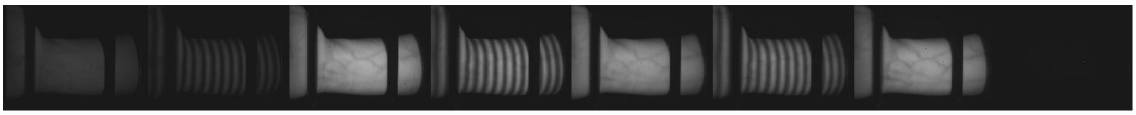

Figure 7. Measured image for our SFDI system (average of 10 images, Brightness +20%, Contrast +20%)

5. CONCLUSION

We proposed the three-band SFDI method using an 8-tap CMOS image sensor and the Hilbert transform. We successfully measured DC and sine images for three main wavelengths and one DC image for the additional 4th wavelength using the proposed method. Improvement of the signal-to-noise ratio of the new sensor is an important issue for accurate tissue measurement.

ACKNOWLEDGEMENT

This work was supported in part by JSPS KAKENHI Grant Number 18H05240 and 21H04557. Drs. Durkin and Kennedy thankfully recognize support from the NIH, including the National Institute of General Medical Sciences (NIGMS) Grant No. R01GM108634. The content is solely the responsibility of the authors and does not necessarily represent the official views of the NIGMS or NIH.

REFERENCES

[1] D. J. Cuccia et al., "Quantitation and mapping of tissue optical properties using modulated imaging," J. Biomed. Opt. 14(2), 024012 (2009).

[2] Kazuki Takada et al., "Demonstration of 3-band spatial frequency domain imaging using an 8-tap CMOS image sensor resistant to subject motion and ambient light," Proc. SPIE. 11951, Design and Quality for Biomedical Technologies XV, 1195106 (2022).

[3] Y. Shirakawa, K. Yasutomi, K. Kagawa, S. Aoyama, and S. Kawahito, "An 8-tap CMOS lock-in pixel image sensor for short-pulse time-of-flight measurements," MDPI Sensors, Vol. 20, Issue 4, Article 1040 (2020).

[4] K. P. Nadeau, A. J. Durkin, and B. J. Tromberg, "Advanced demodulation technique for the extraction of tissue optical properties and structural orientation contrast in the spatial frequency domain," Journal of Biomedical Optics, Vol. 19, No. 5, 056013 (2014).
[5] S. Kawahito, G. Baek, Z. Li, S. Han, M. Seo, K. Yasutomi and K. Kagawa, "CMOS lock-in pixel image sensors with lateral electric field control for time-resolved imaging," *International Image Sensor Workshop*, 10.06, pp.1417-1429 (2013).
[6] D. J. Cuccia, F. Bevilacqua, A. J. Durkin, F. R. Ayers, and B. J. Tromberg, "Quantitation and mapping of tissue optical properties using modulated imaging," Journal of Biomedical Optics, vol. 14, no. 2, (2009).
[7] A. Mazhar, S. Dell, D. J. Cuccia, S. Gioux, A. J. Durkin, J. V. Frangioni, and B. J. Tromberg, "Wavelength optimization for rapid chromophore mapping using spatial frequency domain imaging," Journal of Biomedical Optics, Vol. 24, No. 4, pp. 639-651(2009).
[8] A. Ponticorvo et al., "Spatial Frequency Domain Imaging (SFDI) of clinical burns: A case report," Burns Open, Vol. 4, Issue 2, pp. 67-71(2020).